Processes in model slopes made of mixtures of wettable and water repellent sand: implications for the initiation of debris flows in dry slopes

Sérgio D.N. Lourenço[1], Gong-Hui Wang[2], Toshitaka Kamai[2]

[1] Department of Civil Engineering, The University of Hong Kong, Pokfulam Road, Hong Kong SAR; lourenco@hku.hk; +852 3917 2672; corresponding author

[2] Disaster Prevention Research Institute, Kyoto University, Gokasho, Uji 611-0011, Japan

Abstract

Debris flows in slopes initially dry, such as post-wildfire debris flows, are initiated by surface runoff and sediment bulking due to reduced infiltration. Soil water repellency, extreme dry soils, and loose, cohesionless materials influence their initiation. The exact link between these features, the resulting infiltration processes and the initiation mechanism of a debris flow remains unclear. Here, we examine the relation between soil particle wettability and slope processes in physical models. Flume experiments were conducted in 10% increments of mass ratiosof wettable to water repellent sand, subjected to artificial rainfall with monitoring of soil water content, pore water pressure, sediment and water discharge and failure mode. To date, wettability was considered only for the water repellent end, because it reduces infiltration, enhancing surface runoff. This study demonstrates that slight wettability changes, in the full wettable to water repellent range, impact a variety of slope processes. The two extremes, fully wettable and water repellent gave opposite responses, retrogressive slides for infiltration-initiated in wettable sand and erosion by surface runoff in water repellent sand. The transition was dominated by surface runoff and preferential flow, yielding a combination of erosion and slides. From the tests, a continuous capping effect generated by water repellency was a necessary condition for erosion and sand bulking i.e. the generation of runoff-initiated debris flows. The sensitivity of the model slope response to artificial rainfall was particularly acute at high ratios of wettable to water repellent sand. For mixtures above a critical ratio of wettable to water repellent sand, the measurements with an index test revealed a fully wettable material despite differences in the infiltration, saturation and pore water pressure built-up trends. Implications for post-wildfire debris flows and debris flows in slopes initially dry in general are discussed.

Keywords

Debris flows, soil particle wettability, wildfires, dry soils, flume tests

1. Introduction

Debris flows are often mobilized by a shallow slide in response to infiltration, saturation and rising pore water pressures (Ellen and Fleming, 1987). However, this mechanism does not hold for slopes affected by wildfires, where debris flows are triggered by surface runoff and sediment bulking in response to short duration, high intensity rainfall events (Wondzell and King, 2003, Cannon and Gartner, 2005). In such cases, the key factor controlling infiltration is soil water repellency, the others being extreme dry soils (Moody and Ebel, 2012) and sealing of pores by ash (Mallik et al., 1984, Gabet and Sternberg, 2008, Woods and Balfour, 2010). Soil water repellency (Figure 1) develops with the presence of organic water repellent substances (generated by the wildfires but also naturally occurring) and when the soil becomes dry (Doerr et al., 2000), and is quantified via the contact angles of water drops in contact with the soil, wettable soils have contact angles <90° and water repellent soils >90°. The general term 'soil particle wettability' includes wettable and water repellent soils.

The ninety-degree contact angle represents a threshold at which the mechanical and hydraulic behavior of the soil, and therefore the slope response, is expected to change. The significance of the threshold can be demonstrated with Young-Laplace equation, which states that soil particle wettability (θ) relates to matric suction (s), and the radius (r) and surface tension (T) of the water menisici via $s = 2T\cos\theta/r$ (Fisher, 1926). Matric suction, which controls unsaturated soil behavior (Fredlund and Rahardjo, 1993), will be the highest for low contact angles (wettable soils) and the lowest for high contact angles (water repellent soils). This suggests that soils with high contact angles are likely to be mechanically weaker, therefore more prone to landslides. Byun et al. (2011) showed decreasing friction angles for synthetic water repellent soils. For the capillary rise in unsaturated soils, the same equation can be rewritten as, $h = \cos\theta 2T/r\rho g$, where h is the capillary rise, ρ is the density of water, and g the gravitational constant. Water will only rise (or infiltrate) for contact angles <90°. For

contact angles >90°, water will only infiltrate when the water-entry pressure is exceeded (the height of water above the water repellent surface).

Soil wettability however is a dynamic property, sensitive to soil-atmosphere interactions. Soil wettability depends on a critical water content: soils are water repellent for a water content lower than the critical and wettable for a water content higher than the critical (Dekker et al., 2001). Recent work has also shown that the soil water retention is affected by soil wettability. Soils with contact angles <90° have reduced water retention i.e. they are drier than an equivalent wettable soil when dried to the same suction (Arye et al., 2011, Lourenço et al., 2015). Importantly, wettability of natural soils is time-dependent, it may decay or enhance with time and switches from wettable to water repellent, and vice-versa, may also occur with time (Morley et al., 2005) and, it has a patchy distribution in natural soils with wettable and water repellent regions spread across the ground (Granged et al., 2011, Jackson and Roering, 2009).

Given the variability of soil wettability, both in time and space, and its threshold-dependent behavior, addressing its role on debris flow initiation is a challenge still to be undertaken. Moreover, debris flow initiation has been documented for the wettable and water repellent ends with little appreciation for the slope response at the transition wettable to water repellent, for instance, for situations where soils may be slightly water repellent.

Here, through a series of physical experiments we document the role of soil particle wettability in the transition from infiltration to runoff-triggered debris flows by considering the whole wettability spectrum, from wettable (<90°) to water repellent(>90°), by mixing the same material to different ratios of soil with and without water repellent substances. This will reveal whether the transition between runoff and infiltration-initiated debris flows is gradual or threshold-controlled (90°) and will provide an insight into the various processes. To minimize other effects, differences between the experiments will be exclusively due to

changes in the affinity of the particle surfaces' for water, with all tests starting under the same initial physical conditions (e.g., material, grain-size distribution and density).

This study arises from a context of post-wildfire debris flows, but the results could be applicable to debris flows in some forested areas (where soils are likely to develop water repellency) (Doerr et al., 2006) and to debris flows in dry soils in general, those likely to be initiated by first-time rainfall events at the end of the dry season or after dry weather spells (Coe et al., 2008). Runoff-initiated debris flows linked to fully wettable, saturated soils are not covered here.

2. Materials and Methods

2.1. Wettability treatment

To induce and adjust the wettability level, the initial strategy was to use natural oily water repellent substances because they simulate natural water repellent substances more closely, allow switches from wettable to water repellent (and vice-versa) and take into account the time-dependency of soil particle wettability (the contact time with water) (Morley et al., 2005). However, as the laboratory procedures are time-consuming and large amounts of treated material were required, permanent water repellent coatings by silanization (i.e. a synthetic water repellent treatment) were used instead. Despite being artificial, permanent water repellent coatings have also been used in other soils studies (Liu et al., 2012). Note that, in these experiments, we name wettable soils those without water repellent substances and water repellent soils those with water repellent substances.

In this study water repellency was induced by treatment with dimethyldichlorosilane (DMDCS) and the wettability level adjusted by mixing wettable and water repellent material to different proportions by mass. The fully wettable sample was non-treated and the fully water repellent sample made of 100% treated material. This could constitute an advantage,

since water repellency is characterized by spatial variability or patchy distribution both vertically and horizontally (Granged et al., 2011) meaning water would preferably flow through the wettable particles. This co-existence of wettable and water repellent particles has been named fractional wettability (Beatty and Smith, 2010).

To avoid material variability and as post-wildfires debris flows occur in granular soils, a medium-sized industrial silica sand was used (SS#7). SS#7 is a uniform, fine silica sand with mean grain size (D_{50}) of 0.13 mm and uniformity coefficient (U_c) of 2.1. The maximum void ratio (e_{max}) is 1.23. The grain size distribution is shown in Figure 2 and material properties in Table 1. This material has also been used in numerous laboratory studies on the mobility of landslides (Wang and Sassa, 2003).

To induce contact angles >90°, the material was removed from the bags, in its natural wettable state, and mixed in a fume hood with a glass beaker and glass rod in portions of 500g of sand to 0.5 ml DMDCS. The treatment was complete after 5 minutes mixing. The treated material was then stored in a large bin until further use.

To prepare the mixtures, the fully water repellent sand was mixed with the wettable sand (freshly removed from the bags) at the following proportions by weight (w = wettable, wr = water repellent): 100% w; 90% w + 10% wr; 80% w + 20% wr; 70% w + 30% wr; 60% w + 40% wr; 50% w + 50% wr; 40% w + 60% wr; 30% w + 70% wr; 20% w + 80% wr; 10% w + 90% wr; 100% wr. Since temperature is known to influence soil particle wettability (Atanassova and Doerr, 2011), no oven drying was conducted prior or after the treatment. Residual water content, which could have been present in the samples prior the treatment or the flume tests, was not measured.

To assess soil particle wettability, the Water Drop Penetration Time test (WDPT) was conducted with a sample of approximately 50g immediately before the flume test. The WDPT is an index test, widely used in soil science in sandy samples (Doerr et al., 2006). The

WDPT quantifies the persistence of water repellency i.e. its time decay. The WDPT consisted in a placing water drops (volume 10 µl, 6 repeats) and timing its complete penetration. For a wettable sand, water penetrates immediately; water repellent substances delay or completely impede infiltration. Based on the penetration times, the samples were classified according to the wettability classes provided by Doerr et al. (2006).

One further sample was collected from each mixture, sealed in a plastic and transported to Cardiff University (UK) one month later to measure the apparent contact angles. The contact angle is a physical parameter quantifying wettability and widely used in surface science (Bachmann et al., 2000). By means of the sessile drop method, three drops of 10 µl were placed on a layer of sand for each mixture, a video recorded with the goniometer (DSA25, Kruss) and the first contact angle, measured on the left and right-hand side of the drop from the time-sequence.

2.2. Model set-up and instrumentation

An important initial question was whether debris flows in soils of different wettability could be generated on a laboratory scale. Debris flows have been induced in the laboratory in metric and centimetric sized models, to investigate their initiation and post-failure dynamics (e.g. Iverson, et al., 2011, Wang and Sassa, 2001). Also, soil water repellency or wettability changes develop at very shallow depths (few centimeters) (Doerr et al., 2000). Therefore, no exact scale modelling (as in a centrifuge) has been attempted here. Careful observations and monitoring the response of the wettable/water repellent mixtures to rainfall were judged at least qualitatively similar, in terms of dominant processes, to the field.

To test the relation between the failure and infiltration mode to soil particle wettability, we carried out 11 experiments in a glass-sided 1.5 m long, 45 cm high and 29.75 cm wide flume. The bottom of the flume was impervious, covered with coarse sand paper (average particle

size 0.5 mm) to increase friction and avoid sliding at the sand-flume interface. The physical model had a trapezoidal shape, 15 cm height, 15 cm wide and 75 cm long. The model slope surface was inclined at the angle of repose of the material (38±1°), (Figure 3). The high length to width ratio (75 cm by 15 cm) was to provide a wider surface in contact with the rainfall and enhance both infiltration (for the wettable mixtures) and runoff (for the water repellent mixtures). The initial slope angle at 38° (angle of repose) was intended to simulate a slope at imminent failure, and potentially, to trigger faster failures.

The sand mixtures were deposited in an air dried state in 5 kg loads until 45 kg was present. The 5kg loads were dropped from a bucket from a height of ~5 cm across the length of the model. For each deposit, the surface was gently spread with a ruler in a single layer until covering the area of the model. This resulted in a layer thickness of around 1 cm for the bottom layers, reaching 2 cm at the top (due to the trapezoidal shape of the model). No compaction was conducted in order to achieve a very loose condition. Before each test, the mass, volume and model angles (38±1°) were measured to obtain the void ratio (1.17±0.04). The water content was not measured and assumed zero. Failure was induced by artificial rainfall, by means of one nozzle with pressure control; rainfall intensity was measured for each test. The pressure of the tap water was adjusted manually so that the rainfall intensity was similar for all tests. The height of the nozzle was also adjusted so that the radial spray exceeded the width of the model but not the length (or the water discharge would be higher). Importantly, the wetting front advance in the 100% wettable tests was used to assess how uniform was rainfall across the model. A wetting front advance parallel to the surface implied uniform rainfall intensity across the model (as shown in Figure 6d). Overall, the rainfall intensity was 34±7 mm/h. As the model was being built, four nests made of soil moisture sensors and pressure transducers were set up to capture the spatial evolution of infiltration and pore water pressure generation. The nests were placed at 5 cm depth and 10 cm depth.

The soil moisture sensors (EC-5, Decagon Devices) measured the volumetric water content and the pressure transducers (PGM-02 kg, Kyowa, maximum capacity 20 kPa) the positive pore water pressure. Both were calibrated in the same material at different water contents (soil moisture sensors) and increasing head of water (pressure transducers). The pressure transducers were fitted with a cap with a small orifice (diameter 0.12 cm), and the gap inside the cap filled with water. The air entry value was estimated at 0.24 kPa (using Young-Laplace equation) suggesting the reservoir would desaturate when in contact with the sand. Therefore, a delay in the pore water pressure increase due to air bubble formation is possible. The pressure transducers sample 10 measurements per second and the soil moisture sensors 1 measurement per minute. Since soil particle wettability is influenced by environmental parameters (Doerr et al., 2002), the ambient temperature and Relative Humidity were recorded before each test.

The failure mode (and infiltration process) was followed visually by recording the whole failure sequence. The video camera was set on the side, oblique to the model in an elevated position to capture both the sides and top surfaces of the model (Figure 3). Video recordings were always conducted from the same side of the flume.

Sand and water discharge were measured at the bottom of the flume with a sieve (aperture 63 μm) and bucket. Since the physical model occupied the top 75 cm of the flume, a plastic sheet was placed from the bottom of the model until the end of flume in order to drain the water and sand (Figure 3). The plastic sheet was effective in the drainage of water, when it reached the toe it would flow out of the flume within ~3 seconds. However, there was a delay in the discharge of sand, as it would accumulate rather than drain out. Therefore, for water discharge, the timing is similar to that at the toe of the model while for the sand discharge there is a delay that could not be quantified.

The initial model conditions and environmental laboratory parameters are shown in Table 2. The initial void ratio was high (1.17±0.07) but lower than the e_{max} for this material (1.23), with the exception of test 1 with 100% wettable sand (void ratio was 1.24 which is likely to reflect experimental error). This was the highest initial void ratio possible to achieve with the model preparation method. Rainfall intensity was 34±7 mm/h, and the temperature and Relative Humidity, ~27.5 ±0.5°C and 86±6%, respectively (Table 2). The flume tests were conducted in a temperature controlled room at 28°C. The temperature and Relative Humidity were kept elevated during the test to match the outside weather conditions (hot and humid at the time) and avoid large diurnal fluctuations (the temperature control would switch off automatically).

Typically, the sand treatment was conducted in the morning, the flume set-up by mid-day and the full test with the artificial rainfall later in the afternoon. Each flume test did not exceed 35 minutes. The flume tests were stopped when a steady state condition was reached or all instrumentation had been severely disrupted by the deformation of the model. The flume was then cleaned, the material disposed (no sand was re-used), and all flume surfaces wiped dry.

Data analysis was conducted, firstly by calibrating all raw data, followed by synchronizing the times for all datasets. In total there was five datasets timed separately: the soil moisture sensors and pressures transducers used separate data loggers, all ten test were filmed in a single file, sand and water discharge measurements, and hand notes of special events or features during the tests. All datasets were zeroed based on the time of the rainfall start, since for the water repellent mixtures surface runoff would start immediately with rainfall. The infiltration and failure modes were based on the video recordings and the sand and water discharge measurements taken at discrete times.

3. Results

3.1. Wettability threshold

Soil particle wettability was the first parameter to be measured. According to the WDPT data, the transition in soil particle wettability for the different mixture ratios was abrupt, rather than linear or gradual, with a threshold at 50w+50wr (Figure 4a). Mixtures from 100 % wettable to 60 % wettable were fully wettable i.e. the water drop would penetrate immediately, followed by a transition for 50 % wettable and 40 % wettable, and ending in extreme water repellency for 30 % wettable until 100 % water repellent.

The apparent contact angles measured by the sessile drop method did not agree with the WDPT data. All mixtures became more water repellent with contact angles in the range 101°-148° except the wettable sample at 9.9° (Figure 4b). We assumed the two parameters would agree, at least, for the water repellent soils with high contact angles and long WDPTs. Reasons for this increased water repellency include: (1) the transport and shaking of the samples for the contact angle measurements could have led to further surface reactions by any residual DMDCS remained in the sample, (2) the contact angles were conducted in substantially cooler and drier conditions (temperature ~ 19°C, Relative Humidity ~ 50%) and, (3) water repellency is known for being time-dependent (Morley et al., 2005).

Despite the empirical nature of the WDPT, we assume it to provide a reliable account of soil particle wettability because it was conducted under the same environmental conditions as the flume tests. We therefore use it in our analysis rather than the apparent contact angles.

To assess the stability of the water repellent condition (whether it changes with time or not), both the WDPT and contact angles were measured with time for the 100 % water repellent sand samples. Figure 5a shows the apparent contact angle with time. For 3 seconds, the droplets in Figure 5b remained stable at 107° without infiltrating. Based on the WDPT data, the drops remained stable for ≥18000 seconds (Figure 4a). In summary, the water repellent

condition was stable, at least, for the duration of the experiments and the behavior observed attributed to the different wettability levels rather than wettability changes during the tests.

3.2. Model slope processes as a function of soil particle wettability

3.2.1. Rational for data interpretation

Three datasets were produced: (1) failure mode and infiltration depth and patterns; (2) volumetric water content and pore water pressure; and (3) water and sand discharge. All these are presented in time series. The flume tests started with the wettable untreated sand followed by tests in 10% increments until 100% water repellent. The wettable sand is the benchmark condition to which all the other tests are compared.

Overall, the flume tests revealed an acute sensitivity to soil particle wettability. The extremes (wettable vs water repellent) provided opposite responses, infiltration-dominated processes for the wettable mixtures (100% and 90% wettable) and runoff-dominated for the water repellent mixtures (0% to 30% wettable). In between, there was a combination of processes.

The main slope processes were identified for the 11 tests and, for the sake of presentation in this paper, the tests were grouped in sand mixtures which exhibited similar behavior and characteristics. The classification of soil wettability by Doerr et al. (2006) was adopted and the groups split into wettable (strong), wettable (weak), moderate to severe, and extreme. The split into two wettable states (strong versus weak) was necessary to account for differences in the infiltration mode (wetting front versus preferential flow). In our analysis and interpretations, we link the volumetric water content and video recordings to the infiltration mode and saturation process; the failure mode from the video recordings to the pore water pressure data (rising pore water pressures trigger failure); while the sediment and water discharge is compared to all data. One representative test from each group, i.e. sharing similar characteristics, is presented next. Time-elapsed photographs and the time-series data from the

remaining tests are available in the supporting information. To allow comparison between the different time-series datasets, all figures have the same axis scales.

3.2.2. Wettable sand (strong) mixture

The time series results for the 100% wettable sand are shown for the pore water pressure in Figure 6a, volumetric water content in Figure 6b, water and sand discharge in Figure 6c and failure mode and infiltration from the video snapshots in Figure 6d. From the 11 tests, the descriptions below are applicable to tests 100w and 90w+10wr (Figure A1 in supporting information).

The photographs show a wetting front, parallel to the surface travelling downward. No surface runoff was observed, all rainfall infiltrated. These observations were corroborated by the volumetric water content data, with a sudden increase at 4 minutes for the shallow soil moisture sensors (nests 1 and 2) followed by the deeper soil moisture sensors (3 and 4).

Pore water pressure increase initiated at 14 minutes at the transducers near the slope (nests 1 and 3) propagating towards the back of the model. Eventually, the thinning of the model near the toe allowed water to saturate and generate positive pore water pressure from the toe (transducers 1 and 3) towards the back of the model (transducers 2 and 4). The drop in pore water pressure in transducers 1 and 3 near the toe, at 18 minutes, matches the onset of failure from the video recordings, through a series of retrogressive slumps. A similar drop is documented for the back transducers (2 and 4) as the slumps approach their location. Rather than dilation-linked (pore-size increase in dense materials), we interpret the pore water pressure drops as a lowering in the water table due to the shortening of the physical model length.

Assuming saturated vertical downward flow, the pore water pressure generation would have been lower than hydrostatic. However, all transducers measured maximum pore water

pressures in excess of hydrostatic, 1.0 kPa for the lower transducers. This was interpreted as a fast sand contraction (volume reduction in loose materials under reduced drainage) with pore water being expelled from the water-saturated pores generating pore water pressure. Collapse upon wetting is typical of very loose granular soils when wetted for the first time (Houston et al., 2001).

Evidence of air entrapment or pore air pressure generation that could delay infiltration was not observed (Siemens et al., 2013). No specific geomorphic features were observed during infiltration indicating air release (e.g. pockmarks). Failure initiated in the toe, so it is possible trapped air (if any) would be released from the toe area.

For the water and sand discharge, up to 17 minutes, only water had discharged at the end of the flume. During this time, sand would accumulate at the toe of the model. With the continuous rainfall and retrogressive slumps the model eventually reached an equilibrium slope angle of the flume's extension.

3.2.3. Wettable sand (weak) mixture

The selected representative test for predominantly wettable sand was the 60w+40wr. Despite having 40% water repellent sand, according to the WDPT it is still classified as wettable. The descriptions apply to tests with 80%, 70% and 60% wettable sand. The time series results for the 60w+40wr are shown in Figure 7a for the pore water pressure, Figure 7b for the volumetric water content, water and sand discharge are in Figure 7c, and snapshots of the video recordings for the failure mode and infiltration process in Figure 7d. The data sets for the 80% and 70% wettable sand are provided in Figure A2 and Figure A3, respectively, in supporting information.

The video recordings show temporary ponding of water at the surface, followed by infiltration. Rather than a wetting front parallel to the surface, preferential flow or fingering

was observed throughout the tests. Preferential flow is a key feature of water repellent soils (Ritsema et al., 1998). It was also observed that water would advance both downward and laterally along horizons. We speculate these horizons could correspond to more water repellent horizons possibly a result of poor mixing of wettable and water repellent sand. Four major fingers can be observed in Figure 7d. The infiltration mode was validated by the soil moisture data, with the upper soil moisture sensors (1 and 2) increasing before sensors 3 and 4.

Failure initiated at 8:30 minutes at the toe of the model by small retrogressive slumps. Dry sand pockets were visible as failure progressed. From the video recordings, water and sand appear flowing out of the model, while portions of sand remained dry within the model. A possible scenario is that water travelled along preferential paths downward until reaching the bottom of the flume followed by lateral outward flow. This is compatible with the timing for the pore water pressure increase for transducer 2 at the top and back of the model (12 minutes) and transducer 4 at the back and bottom of the model (17 minutes), both earlier than the tests at higher proportions of wettable sand. We speculate the fingers observed laterally through the glass, may not extend inwards. They may have developed different shapes and travelled different extents. The response of transducer 1 is not clear. The development of negative water pressure is possible since the water in the cap may have been drawn out of the cap by capillarity, generating a suction effect. However, this response was unique in comparison to all tests, thus not verifiable.

Water and sand reached the bottom of the flume at 7 minutes for water and 12 minutes for sand, earlier than the tests at higher proportions of wettable sand. The sand and water discharge increased linearly until 25 minutes. The test terminated when the model reached an equilibrium slope running the length of the flume.

3.2.4. Moderate to severe water repellent sand mixture

Test 7 with 40% wettable sand and 60% water repellent sand was selected as representative of the predominantly water repellent sand tests. The time series results are shown for the pore water pressure in Figure 8a, volumetric water content in Figure 8b, water and sand discharge in Figure 8c and failure mode and infiltration snapshots of the video recordings in Figure 8d. The wettability for the mixture is classified as moderate i.e. water infiltration is temporarily inhibited. The descriptions apply to tests with 40% and 50% wettable sand (the 50% wettable is in Figure A4 in supporting information).

The time-elapsed photographs show no infiltration in the first 10 minutes. Surface runoff started promptly with the artificial rainfall in the model's steeper slope. By 8 minutes, a rill was formed in the center, enlarging in size both laterally and in-depth. The rainfall continuously depleted the material by surface runoff. No slumps were observed. Both the pore water pressure and volumetric water content measurements revealed a random behavior with no obvious sequence or trends. The pore water pressure suddenly increased followed by dissipation in the shallow transducers (nests 1 and 2). This was followed by the volumetric water content in nest 2 and then 4 and 3. Since the transducers and soil moisture sensors were placed side by side within each nest, we speculate that preferential flow was dominating infiltration with vertical and horizontal pipe flow randomly developing within the model. Both water and sand reached the bottom of the flume within 3.5 minutes.

Upon completion of the test, parts of the model remained fully dry. All the boundaries: glass-sides, top, bottom and the area around the cables were wet with dry sand pockets in-between. It is possible all these interfaces may have contributed to interface flow, since they were more wettable than the surrounding wettable/water repellent mixture.

3.2.5. Extreme water repellent sand mixture

The test presented next was conducted on the 100% water repellent sand. The sand's water repellency classified as extreme, the highest in the scale. The descriptions apply to tests with 90%, 80% and 70% water repellent sand, available as Figure A7, Figure A6 and Figure A5, respectively, in supporting information. The time series results for test 100wr are shown in Figure 9a for the pore water pressure, Figure 9b for the volumetric water content, water and sand discharge in Figure 9c and snapshots of the video recordings for the infiltration and failure mode in Figure 9d.

Throughout the duration of the test, no water infiltrated. All volumetric water contents remained below 0.015. All pressure transducers remained near zero, except for transducer 1, when all the sand was washed out and it got in contact with free water. Surface runoff started simultaneously with the rainfall onset, and developed in a series of rills. Unlike the wettable samples, where an equilibrium slope angle was formed with time, for the water repellent samples, the whole front slope retrogressed backwards with the continuous surface runoff. There was no deposition of material at the toe of the slope, all the material was washed-out. Both water and sand reached the bottom of the flume shortly after the rainfall onset. The relation between both was linear throughout the test.

Upon completion of the test, all the sand remained fully dry, except the upper surface in contact with the atmosphere. No infiltration was observed at the interface sand-glass or cables.

4. Discussion

This study demonstrates that slight wettability changes, in the full wettable to water repellent range, impact a variety of slope processes. Note that all changes were exclusively due to changes in the affinity of the surface of the particles to water. All tests started under the same

initial conditions, and the void ratio was similar for all tests. For instance, a denser packing and a reduction of particle size would have reduced infiltration leading to similar responses as in this study. Figure 10 is a graphic representation of all processes and their dependencies for the 11 sand mixtures, in terms of wettability, failure mode, infiltration mode, volumetric water content, pore water pressure and water – sand discharge.

4.1. Simplified model

We propose that most dry soil slopes in nature occur at different wettability states, with the general response to rainfall controlled by the wettability state. Wettability data to validate this is very limited and mostly related to the water repellent end, and within soil science studies (Bachmann et al., 2008; Doerr et al., 2006). However, there is indirect evidence that dry soils are unlikely to be fully wettable. For instance, contact angles of 0° require flat clean surfaces which do not exist in nature. A series of factors increase contact angles: water menisci movement and velocity (De Gennes, 1985; Hoffman, 1975), microasperities (Taniguchi and Belfort, 2002), impurities and solutes (Fisher and Israelachvili, 1981), organic matter (Chenu et al., 2000), microbial cells (Busscher et al., 2000), surfactants (Karagunduz et al., 2001) including soil type and mineralogy (e.g. Fisher and Lark, 1980). We suggest four wettability classes, the same as in the results section, where each class shares similar attributes. As presented in the Introduction, 90° is assumed the theoretical threshold contact angle at which the hydraulic and mechanical response of the soil changes, below this value particles attract and water infiltrates, and above this value, particles repel and water does not infiltrate. Figure 11 illustrates the responses of slopes to rainfall made of such materials at different wettability states. The settings in the natural and built environment where they could occur are presented.

a. Wettable soil (strong) (<<90°): infiltration by a descending wetting front parallel to the surface; failure initiation by slides. We found no evidence of a parallel wetting

front advance and landslide initiation links in field studies. Most studies are based on spot measurements of pore water pressure and volumetric water content (Li et al., 2004). We assume this response may occur in recent, disturbed deposits (e.g. debris flows deposits) where the particle surfaces are fresh and without organic coatings. Most commonly occurring minerals such as quartz are wettable (Fisher and Lark, 1980).

b. Wettable soil (weak) (<90°): infiltration by preferential flow; failure initiation by sliding. This stage represents, possibly, the most common situation in the debris flows literature. Preferential flow has been widely studied and closely linked to the initiation of debris flows (McDonnell, 1990). May also be representative of long term conditions after a wildfire where wettability was been recovered with the vegetation regrowth (Cannon and Gartner, 2005).

c. Moderate to severe water repellent soil (>90°): limited, local infiltration by preferential flow after a period of time; infiltration initiates when long duration rainfall events overcome the water repellent effect; pore water pressure spikes; failure initiation by surface erosion. Occurs sometime after wildfires (Hubbert et al., 2012) and in some forest soils (Doerr et al., 2006).

d. Extreme water repellent soil (>>90°): complete capping; failure initiation totally driven by surface erosion; water repellent effect only overcome by prolonged wetting or washing out of water repellent horizon. Occurs shortly after wildfires or when the water repellent effect is at its highest (Hubbert et al., 2012).

The scheme above and Figure 11 do not imply soils permanently belong to a particular class and it does not force soils to undergo the sequence a to b to c to d. Changes from one wettability state to the other are possible as soils dry and wet and, changes in wettability state may be gradual or sudden e.g. wettable condition switching to strong water repellent (a to d).

The model does not imply that wettability is the only parameter to be considered in debris flows that initiate in slopes initially dry. Soil water retention is influenced by soil wettability (Arye et al., 2011; Lourenço et al., 2015), so soil water content and matric suction will need to be considered. For infiltration-initiated debris flows, the mechanics will also need to be added. The dependency of shear strength on suction and water content is well known (Escario and Saez, 1986) but the effect of soil wettability will have to be further investigated.

4.2. Sensitivity of slope processes to soil particle wettability

The results suggest that as long as there is some water repellency (water beading up at the surface), no infiltration occurs and debris flows are runoff-initiated. However, in nature this may depend on the rainfall characteristics and the persistency of soil water repellency. Since the long contact of a water repellent soil with water renders the soil wettable, long duration, low intensity rainfall events may overcome the water repellent effects, eventually allowing water to infiltrate and mobilize a discrete mass of soil into a debris flow. The time span of our experiments is too short (up to 30 minutes) and the rainfall intensity rather high (~ 40 mm/h) to consider these time effects. Understanding the relative timescales of soil water repellency decay in relation to rainfall intensity and duration is essential.

Infiltration-initiated debris flows do not depend on the infiltration mode. According to the results, wettable particle surfaces are the necessary condition for water to infiltrate, saturate the ground and mobilize a slide. Retrogressive slumps were observed for tests with 100 % to 60 % wettable sand, but while infiltration was parallel to the surface for the 100 % and 90 % wettable sand mixtures, preferential flow dominated for the 80 % to 60 % wettable sand mixtures. However, a change in wettability at 80 % wettable sand is plausible, but the method used (the Water Drop Penetration Time) may not be sufficiently sensitive to capture the subtle changes.

The data also shows that the pore water pressure built-up behaviour depends on soil particle wettability. For the wettable mixtures with 100 % and 90 % wettable sand, pore water pressure increased from the toe backwards, while for the wettable mixtures with 80 % to 60 % wettable sand (with preferential flow), the increase was random and dependent on the location of the fingers. For the 50 % and 40 % wettable sand, pore water pressure increased in a series of pulses, followed by a slow decrease with time. The pore water pressure pulses appear not to be documented in the literature. We speculate that since the transducers monitor pore water pressure locally, when a vertical pipe reaches a transducer, it generates an immediate increase of pore water pressure equivalent to the head of water in the pipe, as the pipe continues to travel downward or dissipates laterally, the head of water (and pore water pressure) reduces. A pipe is interpreted as a column of water. For the mixtures with less than 30 % wettable sand, the pore water pressure did not change.

Runoff-initiated debris flows are not exclusive of post-wildfire landscapes. Coe et al. (2008) investigated recurrent debris flows in a bare landscape in Chalk Cliffs, Colorado. They measured low volumetric water contents before the debris flows but no information on soil particle wettability was provided. Capra et al. (2010) identified soil water repellency as a mechanism contributing to the generation of lahars in a volcanic landscape in Mexico.

4.3. Experimental limitations

The biggest limitation of this study has been the sole use of the Water Drop Penetration Time. While the WDPT is widely used, it is an empirical measure for the time-dependency of soil water repellency. Measurement of the contact angles, the main physical parameter quantifying wettability, would have been preferred. The Sessile Drop Method was used, but unsuccessfully due to surface wettability changes from sample preparation until

measurement. Other potential methods include the Capillary Rise Method and the Wilhelmy Plate Method (Bachmann et al., 2003).

The maximum sand and water discharge decreased with increasing soil particle wettability (wettable soils discharge less than water repellent soils) (Figure 12). While it is known that wildfires enhance sediment discharge in burned landscapes, it should be noted that for the wettable mixtures, material accumulated between the toe of the model and bottom of the flume. Therefore, the sand discharge could have been higher for the wettable mixtures.

The model slope is made of a water repellent layer-only; this is a simplification of the ground conditions after a wildfire because it does not take into account the double layer structure of the ground (wettable ash on top of the water repellent layer) or the characteristics of the ash (water storage) (Gabet and Sternberg, 2008) and in particular that the water repellent layer is shallow and very thin (1-2 cm). The impervious horizon appears at the surface, either exposed to the atmosphere or underlain a wettable ash layer near the surface (Kean et al., 2011, Moody and Ebel, 2014). The saturated ash may induce a positive head of water, increasing the water-entry pressure, and accelerating wetting of the underlying soil.

The observed continuous retrogressive slides for the predominantly wettable mixtures are a consequence of the initial model conditions, i.e. the long trapezoidal shape with upper and front free surfaces exposed to continuous rainfall. In natural slopes, debris flows in wettable soils initiate from soil slides, which may or may not continue to fail as retrogressive slides.

5. Conclusions

From a series of flume tests at varying ratios of wettable to water repellent sand, the sequence of processes with decreasing soil particle wettability were identified. Overall, the flume tests revealed an acute sensitivity to soil particle wettability. The two extremes, fully wettable and water repellent gave opposite responses, retrogressive slides for infiltration-initiated in

wettable sand and erosion by surface runoff in water repellent sand. The transition was dominated by surface runoff and preferential flow, yielding a combination of erosion and slides. From the tests, a continuous capping effect generated by water repellency was a necessary condition for erosion and sand bulking (i.e. the generation of runoff-initiated debris flows). The sensitivity of the model to artificial rainfall was particularly acute at high ratios of wettable to water repellent sand. Our intention in this paper has been to demonstrate experimentally the importance of soil particle wettability to the initiation of debris flows and spur the need to develop models that can account for such fundamental parameter. Soil particle wettability should not be explored in isolation as demonstrated here, but instead as how it impacts the hydraulic and mechanical properties, their interplay with vegetation, and how the three vary in space and time. To validate these ideas, field wettability data is needed.

Acknowledgements

Financial support for the flume tests and travel costs for the main author were provided by Kyoto University through a long-term research visit grant. Mr. Jiang Yao (DPRI, Kyoto University) assisted with the flume tests in its initial stages and conducted the calibration for the soil moisture sensors. The sand treatment was conducted in Dr. Keisuke Matsushita's laboratory (DPRI, Kyoto University).

References

Arye G., J., Tarchitzky, Chen, Y. 2011. Treated wastewater effects on water repellency and soil hydraulic properties of soil-aquifer treatment infiltration basins. J. Hydrol. 397, 136-145.

Atanassova, I., Doerr, S.H. 2011 Changes in soil organic compound composition associated with heat-induced increases in soil water repellency. European Journal of Soil Science 62, 516-532.

Bachmann, J., Horton, R., Ploeg, R.R. van der, Woche S. 2000. Modified sessile drop method for assessing initial soil-water contact angle of sandy soil. Soil Sci. Soc. Am. J., 64, 564–567.

Bachmann, J., Woche, S.K., Goebel, M.-O., Kirkham, M.B., Horton, R. 2003. Extended methodology for determining wetting properties of porous media. Water Resources Research 39, 12, 1353–1366.

Bachmann, J., Guggenberger, G., Baumgartl, Th., Ellerbrock, R.H., Urbanek, E., Göbel, M.-O., Kaiser, K., Horn, R., Fischer, W.R. 2008 Physical carbon-sequestration mechanisms under special consideration of soil wettability. Special Issue SPP 1090, J. Plant Nutr. Soil Sci., 171, 14–26.

Beatty, S.M., Smith. J.E. 2010. Fractional wettability and contact angle dynamics in burned water repellent soils. Journal of Hydrology 391, 97-108.

Byun, Y.-H., Tran, M.K. Yun, T.S., Lee, J.-S. 2011. Strength and stiffness characteristics of unsaturated hydrophobic granular media. ASTM Geotechnical Testing Journal 35, 1, 1-8.

Busscher, H. J., Weerkamp, A. H., Mei, H. C. van der, Pelt, A. W. J. van, Jong, H. P. De, Arends, J. 2000. Measurement of the Surface Free Energy of Bacterial Cell Surfaces and Its Relevance for Adhesion. App. Environ. Microbiology, 48, 5, 980-983.

Cannon, S.H., Gartner, J.E. 2005. Wildfire-related debris flow from a hazards perspective, M. Jakob and O. Hungr (eds), Debris-flow Hazards and Related Phenomena, 363-385.

Cannon, S.H., Boldt, E.M., Laber, J.L., Kean, J.W., Staley, D.M. 2011. Rainfall intensity–duration thresholds for postfire debris-flow emergency-response planning. Natural Hazards 59, 209–236.

Capra, L., Borselli, L., Varley, N., Gavilanes-Ruiz, J.C., Norini, G., Sarocchi, D., Caballero, L., Cortes, A. 2010. Rainfall-triggered lahars at Volcán de Colima, Mexico—surface hydro-repellency as initiation process. J. Volcanology Geothermal Res. 189, 105–117.

Cerdà, A., Doerr, S.H. 2005. Influence of vegetation recovery on soil hydrology and erodibility following fire: an 11-year investigation. International Journal of Wildland Fire 14, 4, 423-437.

Chenu, C., Bissonnais, Y. L., Arrouays D. 2000. Organic Matter Influence on Clay Wettability and Soil Aggregate Stability. Soil Sci. Soc. Am. J. 64, 1479–1486.

Coe, J.A., Kinner, D.A., Godt, J.W. 2008. Initiation conditions for debris flows generated by runoff at Chalk Cliffs. Geomorphology 96, 270-297.

Dekker, L.W., Doerr, S.H., Oostindie, K., Ziogas, A.K., Ritsema, C.J. 2001. Water repellency and critical soil water content in a dune sand. Soil Sci. Soc. Am. J. 65, 1667– 1674.

De Gennes, P.G. 1985. Wetting: statics and dynamics. Rev. Modern Physics 57, 3, I, 827-863.

Doerr, S.H., Shakesby, R.A., Walsh, R.P.D. 2000. Soil water repellency: its causes, characteristics and hydro-geomorphological significance. Earth-Science Reviews 51, 1, 33-65.

Doerr, S.H., Dekker, L.W., Ritsema, C.J. Shakesby, R.A. 2002. Water repellency of soils; the influence of ambient relative humidity. Soil Sci. Soc. Am. J. 66, 2, 401-405.

Doerr, S.H., Shakesby, R.A., Dekker, L.W., Ritsema, C. J. 2006. Occurrence, prediction and hydrological effects of water repellency amongst major soil and land use types in a humid temperate climate. Eur. J. Soil Sci. 57, 741-754.

Ebel, B., Moody, J.A., Martin, D.B. 2012. Hydrologic conditions controlling runoff generation immediately after a wildfire. Water Resources Research, 48, W03529.

Ebel, B.A., Moody, J.A. 2013. Rethinking infiltration in wildfire-affected soils. Hydrological Processes 27, 1510-1514.

Ellen, S.D., Fleming, R.W. 1987. Mobilization of debris flows from soil slips, San Francisco Bay region, California. In J.E. Costa and G.F. Wieczorek (eds), Debris Flows/Avalanches: Process, Recognition and Mitigation: Geological Society of America. Reviews in Engineering Geology 7, 31-40.

Escario, V., Saez, J. 1986. The shear strength of partly saturated soils. Geotechnique, 36, 3, 453-456.

Fisher, R.A. 1926. On the capillary forces in an ideal soil; correction of formulas by W.B. Haines. J. Agric. Sci., 16, 492-505.

Fisher, L.R. Lark, P.D. 1980. The effect of adsorbed water vapour on liquid water flow in pyrex glass capillary tubes. J. Colloid and Interface Sc. 76, 1, 251-253.

Fisher, L.R. Israelachvili, J. 1981. Experimental studies on the applicability of the Kelvin equation to highly curved concave menisci. Journal of Colloid and Interface Science, 80, 2, 528-541.

Fredlund, D.G., Rahardjo, H. 1993. Soil Mechanics for Unsaturated Soils, John Wiley & Sons

Gabet, E.J., Sternberg, P. 2008. The effects of vegetative ash on infiltration capacity, sediment transport, and the generation of progressively bulked debris flows. Geomorphology 101, 666–673.

Granged, A.J.P., Jordán, A., Zavala, L.M., Bárcenas, G. 2011. Fire-induced changes in soil water repellency increased fingered flow and runoff rates following the 2004 Huelva wildfire. Hydrological Processes 25, 10, 1614–1629.

Hoffman, R.L. 1975. A study of the advancing interface. I. Interface shape in liquid—gas systems. J. Colloid Interface Sc., 50, 2, 228-241.

Houston, S.L., Houston, W.N., Zapata, C.E., C. Lawrence 2001. Geotechnical engineering practice for collapsible soils. Geotechnical and Geological Engineering, 19, 3, 333-355.

Hubbert, K.R., Wohlgemuth, P.M., Beyers, J.L., Narog, M.G., Gerrard, R. 2012. Post-fire soil water repellency, hydrologic response, and sediment yield compared between grass-converted and chaparral watersheds. Fire Ecology 8, 2, 143-162.

Iverson, R.M., Reid, M.E., Logan, M., LaHusen, R.G., Godt, J.W., Griswold, J.G. 2011. Positive feedback and momentum growth during debris-flow entrainment of wet bed sediment. Nature Geoscience 4, 116–121.

Jackson, M., Roering, J.J. 2009. Post-fire geomorphic response in steep, forested landscapes: Oregon Coast Range, USA. Quaternary Science Reviews 28, 11–12, 1131–1146.

Karagunduz, A., Pennell, K.D., Young, M.H. 2001. Influence of a Nonionic Surfactant on the Water Retention Properties of Unsaturated Soils. Soil Sci. Soc. Am. J. 65, 1392–1399.

Kean, J. W., Staley, D.M. Cannon, S.H. 2011. In situ measurements of post-fire debris flows in southern California: Comparisons of the timing and magnitude of 24 debris-flow events with rainfall and soil moisture conditions. Journal of Geophysical Research 116, F04019.

Li, A.G. Yue, Z.Q., Tham, L.G., Lee, C.F. 2004. Field-monitored variations of soil moisture and matric suction in a saprolite slope. Can. Geotech. J. 42, 13–26.

Liu, H., Ju, Z., Bachmann, J., Horton, R., Ren, T. 2012. Moisture-Dependent Wettability of Artificial Hydrophobic Soils and Its Relevance for Soil Water Desorption Curves. Soil Sci. Soc. Am. J. 76, 342–349.

Lourenço, S.D.N., Jones, N., Morley, C., Doerr, S., Bryant, R. 2015. Hysteresis in the soil water retention of a sand-clay mixture with contact angles lower than ninety-degrees. Vadose Zone Journal (accepted)

Mallik, A.U., Gimingham, C.H., Rahman, A.A. 1984. Ecological effects of heather burning: 1. Water infiltration, moisture retention and porosity of surface soil. Journal of Ecology 72, 767–776.

McDonnell, J. 1990. The influence of macropores on debris flow initiation, Quarterly Journal of Engineering Geology and Hydrogeology. 23, 325-331.

Moody, J.A., Ebel, B. 2012. Hyper-dry conditions provide new insights into the cause of extreme floods after wildfire. Catena, 93, 58-63.

Moody, J.A., Ebel, B. 2014. Infiltration and runoff generation processes in fire-affected soils, Hydrol. Processes 38, 3432-3453.

Morley, C.P., Mainwaring, K.A., Doerr, S.H., Douglas, P., Llewellyn, C.T., Dekker, L.W. 2005. Organic compounds at different depths in a sandy soil and their role in water repellency. Aust. J. Soil Res., 43, 239-249.

Ritsema, C.J., Dekker, L.W., Nieber, J.L., Steenhuis, T.S. 1998. Modeling and field evidence of finger formation and finger recurrence in a water repellent sandy soil. Water Resources Research 34, 4, 555-567.

Siemens, G. A., Peters, S. B., Take, W. A. 2013. Comparison of confined and unconfined infiltration in transparent porous media. Water Resources Research 49, 851–863

Taniguchi, M. Belfort, G. 2002. Correcting for surface roughness: advancing and receding contact angles. Langmuir 18, 6465-6467.

Wang, G., Sassa, K. 2001. Factors affecting rainfall-induced flowslides in laboratory flume tests. Géotechnique, 51, 7, 587-599.

Wang, G., Sassa, K. 2003. Pore-pressure generation and movement of rainfall-induced landslides: effects of grain size and fine particle content. Engineering Geology 69, 109– 125.

Wang, Z., Wang, L. Wu, Q.J. 2000. Water-entry value as an alternative indicator of soil water-repellency and wettability. Journal of Hydrology 231–232, 76–83.

Woods, S., Balfour, V. 2010. The effects of soil texture and ash thickness on the post-fire hydrological response from ash-covered soils. Journal of Hydrology 393, 274-286.

Wondzell, S.M., King J.G. 2003. Postfire erosional processes in the Pacific Northwest and Rocky Mountain regions. Forest Ecology and Management 178, 75–87.

Figures and Tables captions

Table 1: Sand properties

Table 2: Testing programme, initial sample and environmental conditions

Figure 1: Schematic representation of interacting water with wettable and water repellent particles (after Bachmann et al., 2008)

Figure 2: Grain-size distribution of Silica Sand #7

Figure 3: Flume set-up. The soil moisture (SM) and pore water pressure (PWP) instrumentation was placed in four nests (1, 2, 3, 4) in two layers at ~5 cm and ~10 cm depth; distance from the glass-sided walls was 15 cm; distance from the back of the flume was 20 cm for the back sensors and 60 cm for the front instruments (RH = Relative Humidity)

Figure 4: Soil particle wettability for the different mixtures. (a) Results from the index test, Water Drop Penetration Time (n=6); the terminology extreme, severe, moderate and wettable follows the classification of the persistency of soil water repellency based on the WDPT by Doerr et al., 2006. (b) Results from the Sessile Droplet Method (n=3)

Figure 5: Contact angle measurements for the 100 % water repellent sand. (a) Stability of the contact angles with time. The three curves correspond to 3 separate measurements where each measurement is the average between the left and right contact angle. Recording started at 0 seconds, drop attached to the grains substrate at ~1 second, reached equilibrium between 1 – 2 seconds and was stable from 2 to 5 seconds. The sampling rate was 40 milliseconds (b) photographs at time = 4 seconds for drop 1, 2 and 3 (drop volume ~12 μl).

Figure 6: Time series data for flume experiment with 100% wettable sand. (a) Pore water pressure. (b) Volumetric water content. (c) Water and sand discharge at the bottom end of the flume. (d) Time-elapsed photographs oblique to the flume; light-dark color in sand denotes dry-saturated areas, respectively (sand height = 14.5 cm)

Figure 7: Time series data for flume experiment with 60% wettable sand and 40% water repellent sand. (a) Pore water pressure. (b) Volumetric water content. (c) Water and sand discharge at the bottom end of the flume. (d) Time-elapsed photographs oblique to the flume; light-dark color in sand denotes dry-saturated areas, respectively (sand height = 14.5 cm)

Figure 8: Time series data for flume experiment with 40% wettable sand and 60% water repellent sand. (a) Pore water pressure. (b) Volumetric water content. (c) Water and sand discharge at the bottom end of the flume. (d) Time-elapsed photographs oblique to the flume; light-dark color in sand denotes dry-saturated areas, respectively (sand height = 14.5 cm)

Figure 9: Time series data for flume experiment with 100% water repellent sand. (a) Pore water pressure. (b) Volumetric water content. (c) Water and sand discharge at the bottom end of the flume. (d) Time-elapsed photographs oblique to the flume; light-dark color in sand denotes dry-saturated areas, respectively (sand height = 14.5 cm)

Figure 10: Model slope processes for the different mixtures, including simplified classification (a, b, c, d) (pwp = pore water pressure, vwc = volumetric water content)

Figure 11: Simplified conceptual model for the initiation of debris flows triggered by rainfall for materials under variable wettability. (a) Wettable soil (contact angle ~0°). (b) Wettable soil (contact angle <90°). (c) Water repellent material (contact angle >90°, when in contact with water remains water repellent for a short period of time). (d) Water repellent material (contact angle >>90°, when in contact with water remains water repellent for a long period of time). Upper row denotes field conditions shortly after the rainfall onset. Middle row is for steady state conditions. Bottom row is on the interaction of meniscus and bulk water with wettable and water repellent particles.

Figure 12: Peak water and sand discharge for the different mixtures

Figures and Tables

Table 1: Sand properties

Physical parameters, symbol (unit)	
Mean grain size, D_{50} (mm)	0.13
Effective grain size, D_{10} (mm)	0.074
Uniformity coefficient, U_c	2.10
Maximum void ratio, e_{max}	1.23
Minimum void ratio, e_{min}	0.70
Specific gravity, G_s	2.63

Table 2: Testing programme, initial sample and environmental conditions

Test nr	% wettable	% water repellent	Slope inclination (°)	Void ratio (e)[1]	Relative Humidity (%)	Temperature (°C)	Water Drop Penetration Time test (s)	Wettability class[2]	Rainfall intensity (mm/h)
1	100	0	38	1.24	-	28	0	Wettable	16.95
2	90	10	37	1.16	76	27	0	Wettable	41.4
3	80	20	39	1.16	88.8	27.9	0	Wettable	37.8
4	70	30	38.5	1.13	95.6	26.4	0	Wettable	36
5	60	40	37	1.18	93.3	27.6	1	Wettable	35.1
6	50	50	39	1.12	86.3	28.1	107	Moderate	36
7	40	60	38	1.14	77.6	27.8	747	Severe	40.8
8	30	70	38	1.16	-	-	14400	Extreme	
9	20	80	37	1.11	82.1	27.4	>18000	Extreme	31.8
10	10	90	35.5	1.25	89.5	27.5	14400	Extreme	30
11	0	100	38	1.18	87.5	27.4	>18000	Extreme	30

[1]From $e = \frac{G_s \rho_w}{\rho_d} - 1$, assuming degree of saturation 0, where G_s is specific gravity, ρ_d is the dry density, ρ_w is the density of water

[2] Following the classification by Doerr et al., 2006

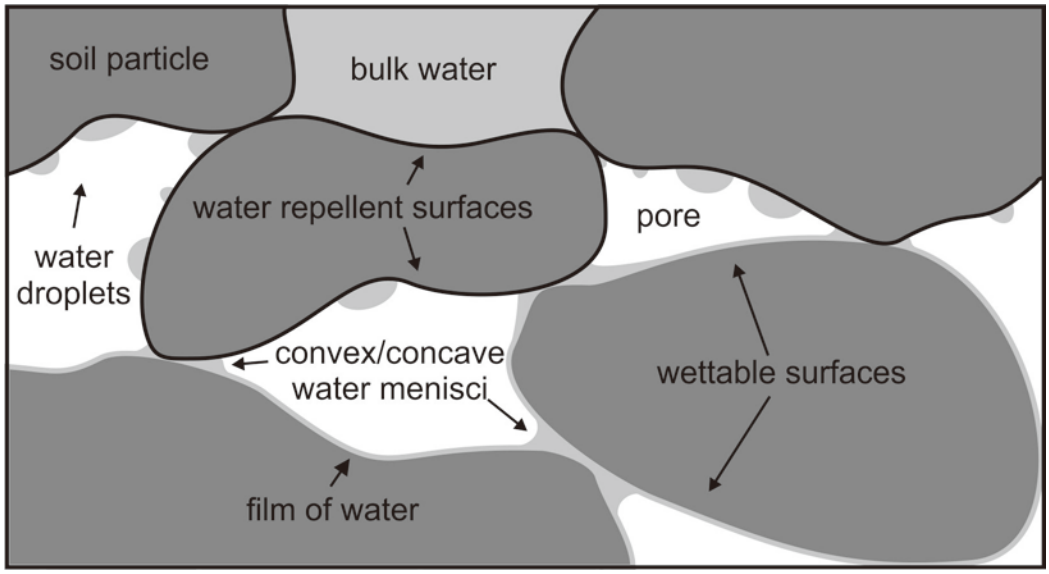

Figure 1: Schematic representation of interacting water with wettable and water repellent particles (*after* Bachmann et al., 2008)

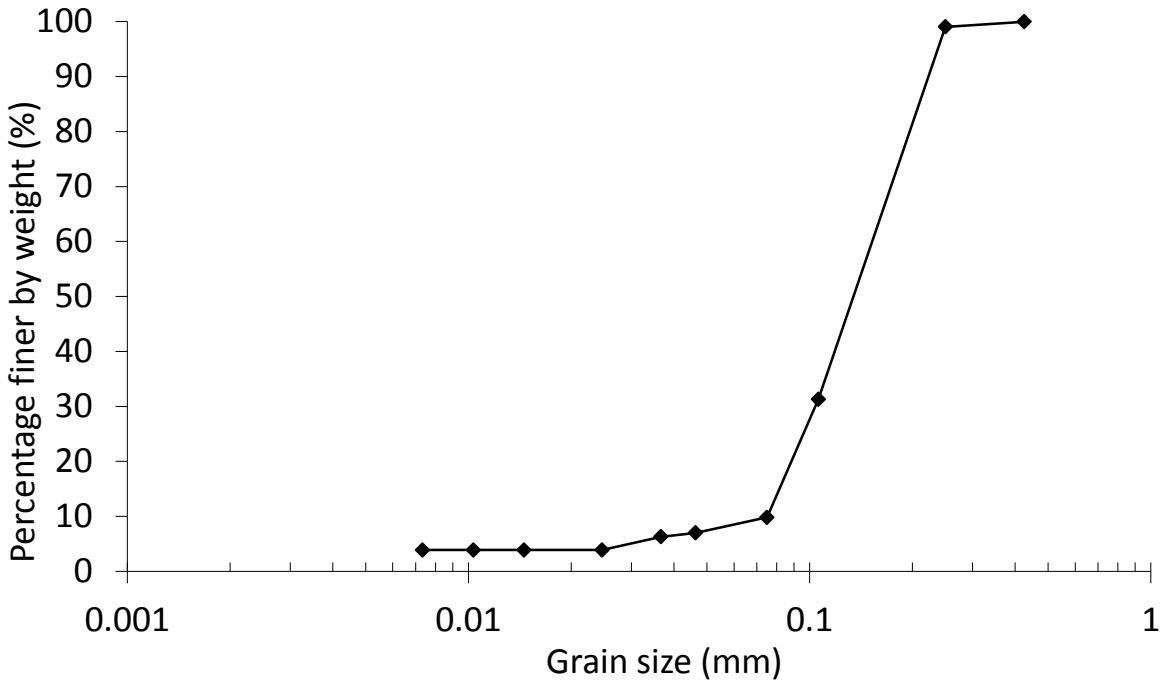

Figure 2: Grain-size distribution of Silica Sand #7

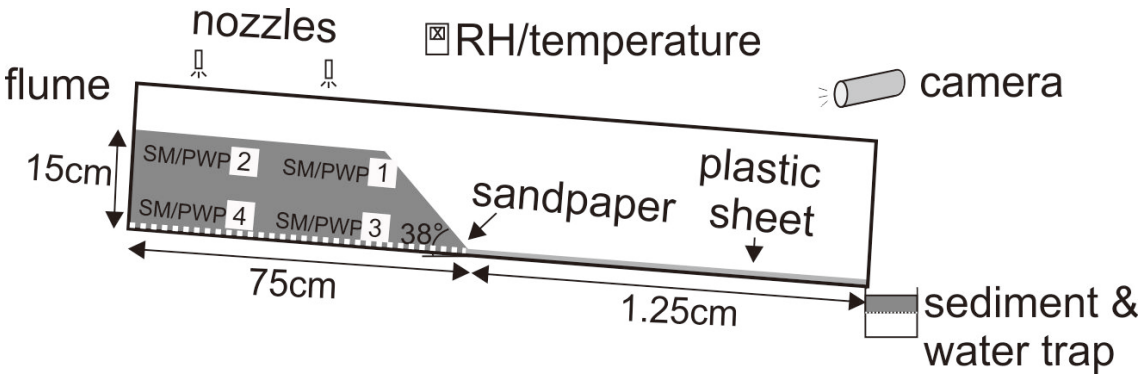

Figure 3: Flume set-up. The soil moisture (SM) and pore water pressure (PWP) instrumentation was placed in four nests (1, 2, 3, 4) in two layers at ~5 cm and ~10 cm depth; distance from the glass-sided walls was 15 cm; distance from the back of the flume was 20 cm for the back sensors and 60 cm for the front instruments (RH = Relative Humidity)

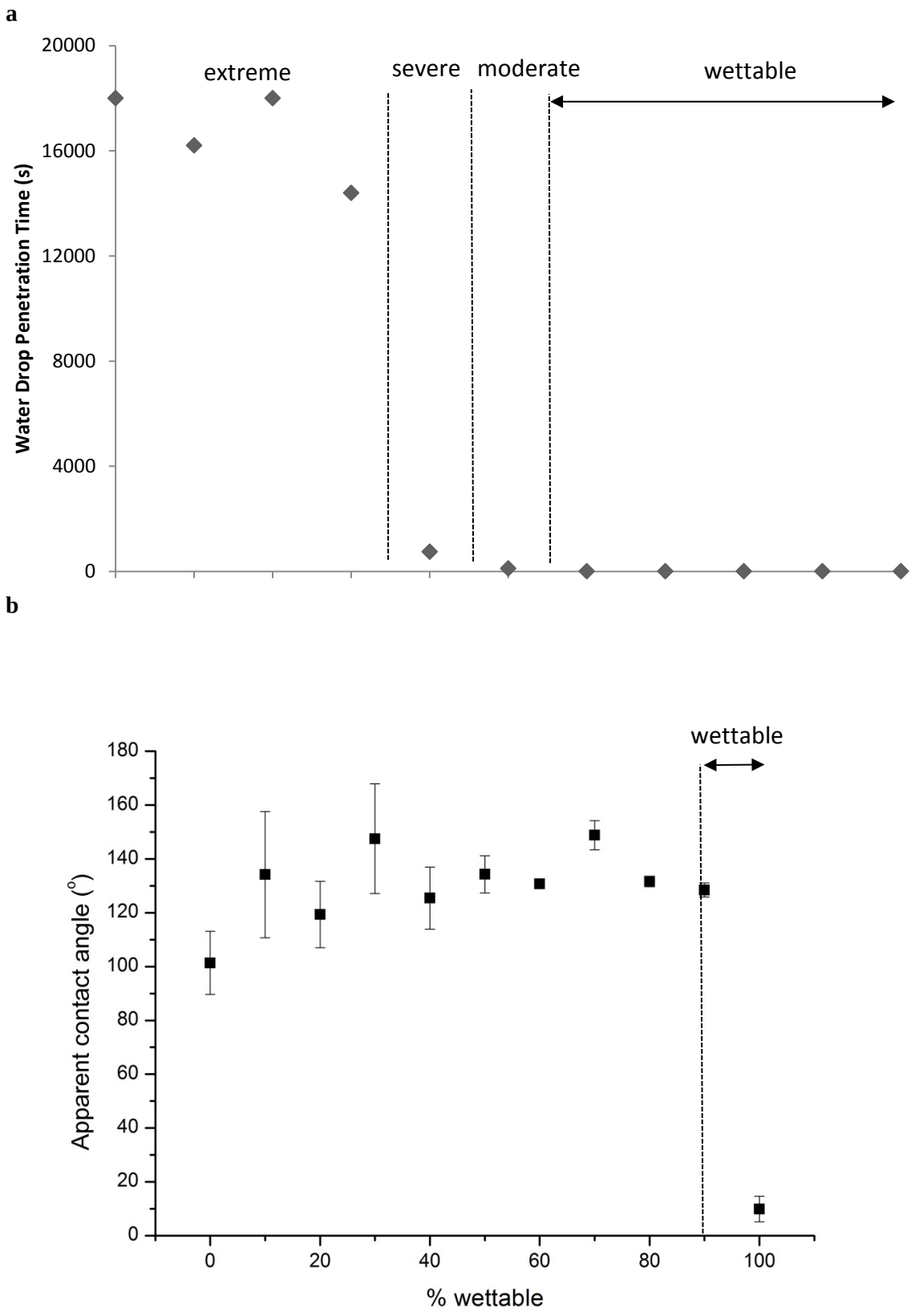

Figure 4: Soil particle wettability for the different mixtures. (a) Results from the index test, Water Drop Penetration Time (*n*=6); the terminology extreme, severe, moderate and wettable follows the classification of the persistency of soil water repellency based on the WDPT by Doerr et al., 2006. (b) Results from the Sessile Droplet Method (*n*=3)

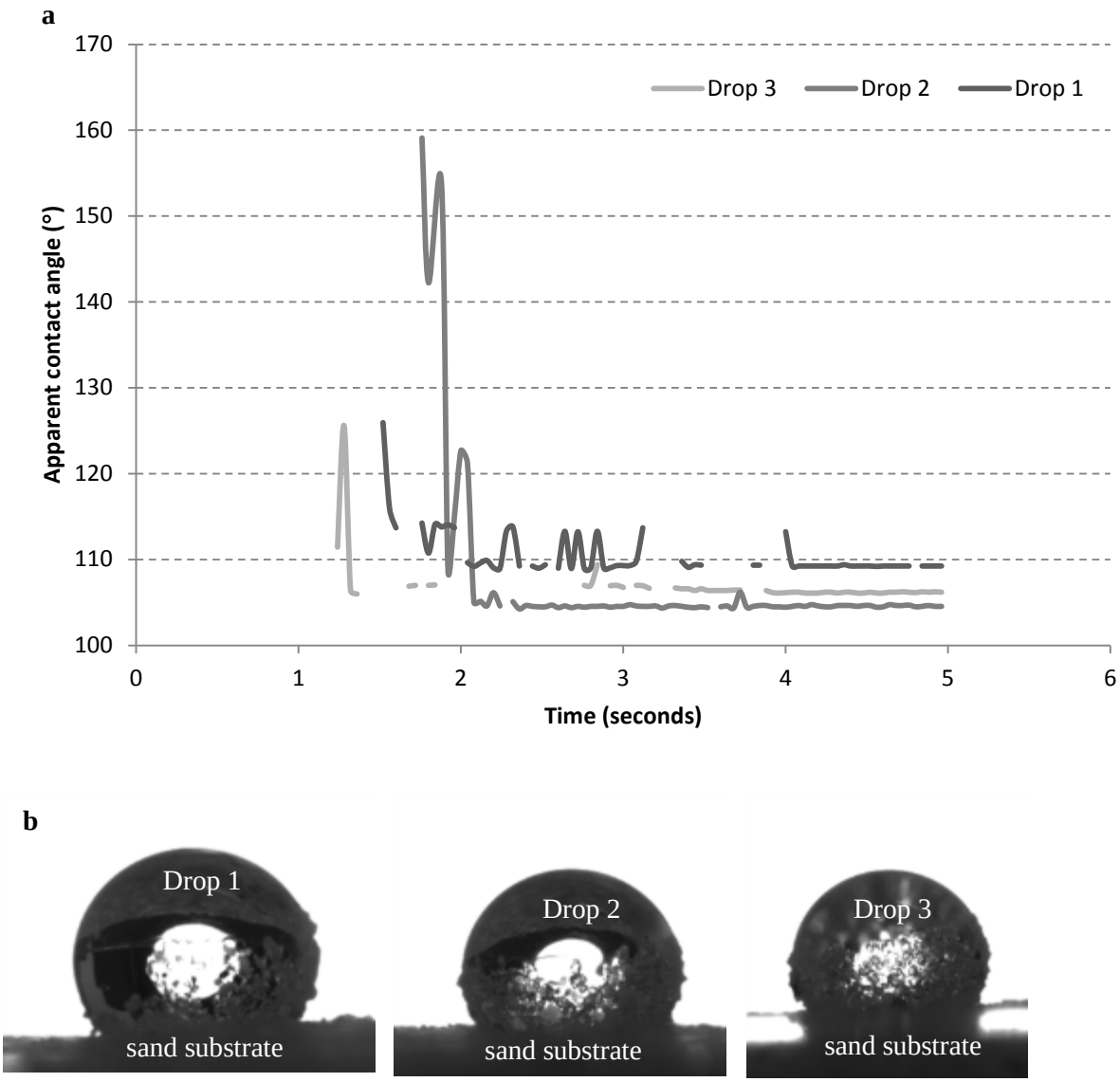

Figure 5: Contact angle measurements for the 100 % water repellent sand. (a) Stability of the contact angles with time. The three curves correspond to 3 separate measurements where each measurement is the average between the left and right contact angle. Recording started at 0 seconds, drop attached to the grains substrate at ~1 second, reached equilibrium between 1 – 2 seconds and was stable from 2 to 5 seconds. The sampling rate was 40 milliseconds (b) photographs at time = 4 seconds for drop 1, 2 and 3 (drop volume ~12 µl).

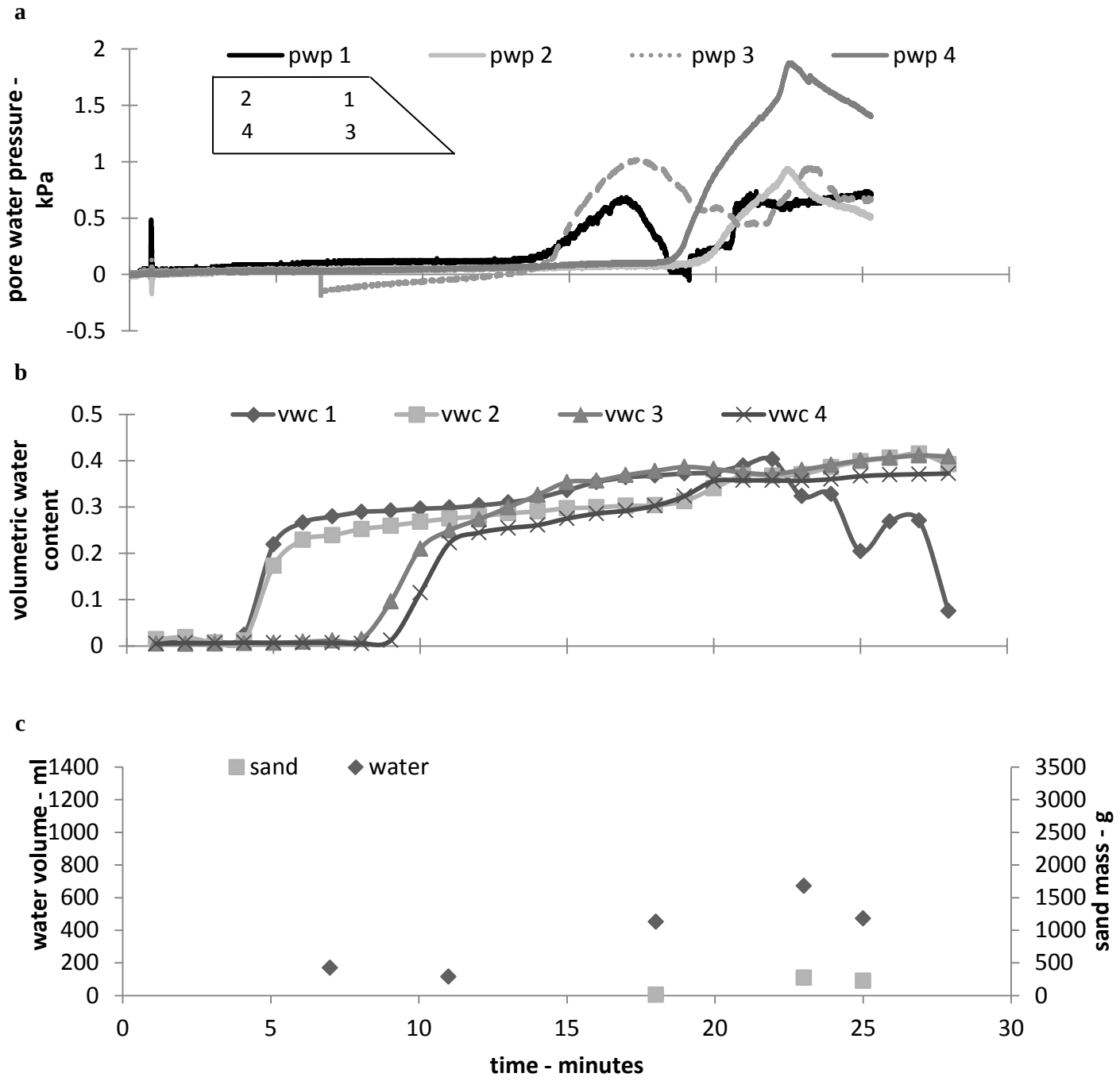
a
pwp 1
pwp 2
pwp 3
pwp 4
2
1
4
3
pore water pressure - kPa
2
1.5
1
0.5
0
-0.5
b
vwc 1
vwc 2
vwc 3
vwc 4
volumetric water content
0.5
0.4
0.3
0.2
0.1
0
c
sand
water
water volume - ml
1400
1200
1000
800
600
400
200
0
3500
3000
2500
2000
1500
1000
500
0
sand mass - g
0
5
10
15
20
25
30
time - minutes

d

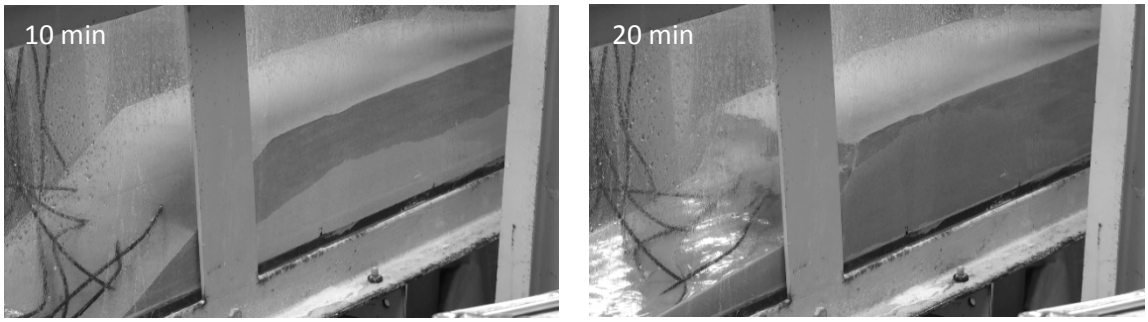

Figure 6: Time series data for flume experiment with 100% wettable sand. (a) Pore water pressure. (b) Volumetric water content. (c) Water and sand discharge at the bottom end of the flume. (d) Time-elapsed photographs oblique to the flume; light-dark color in sand denotes dry-saturated areas, respectively (sand height = 14.5 cm)

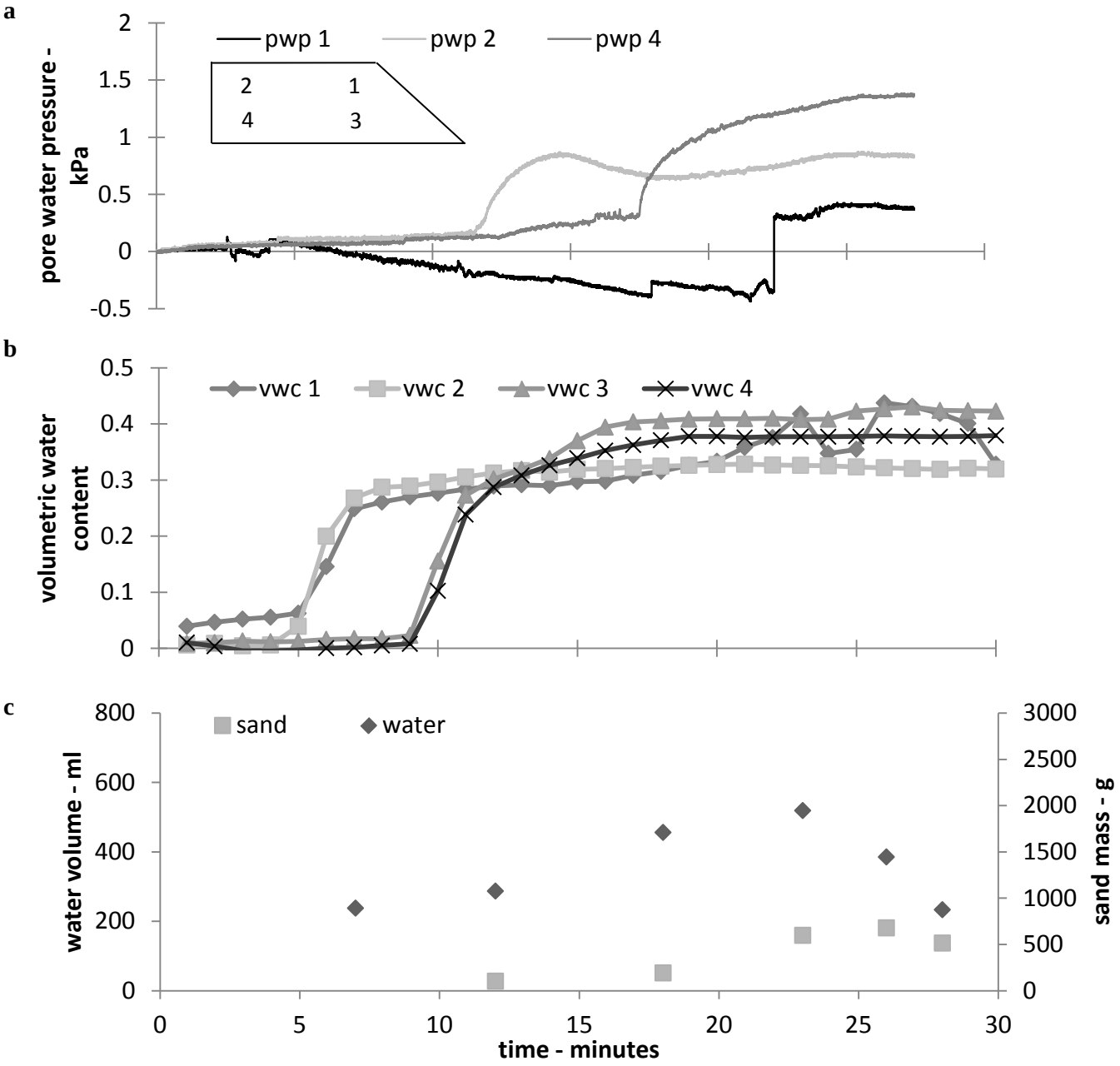
a
pwp 1
pwp 2
pwp 4
2
1
4
3
pore water pressure - kPa
2
1.5
1
0.5
0
-0.5
b
vwc 1
vwc 2
vwc 3
vwc 4
volumetric water content
0.5
0.4
0.3
0.2
0.1
0
c
sand
water
water volume - ml
800
600
400
200
0
3000
2500
2000
1500
1000
500
0
sand mass - g
0
5
10
15
20
25
30
time - minutes

d

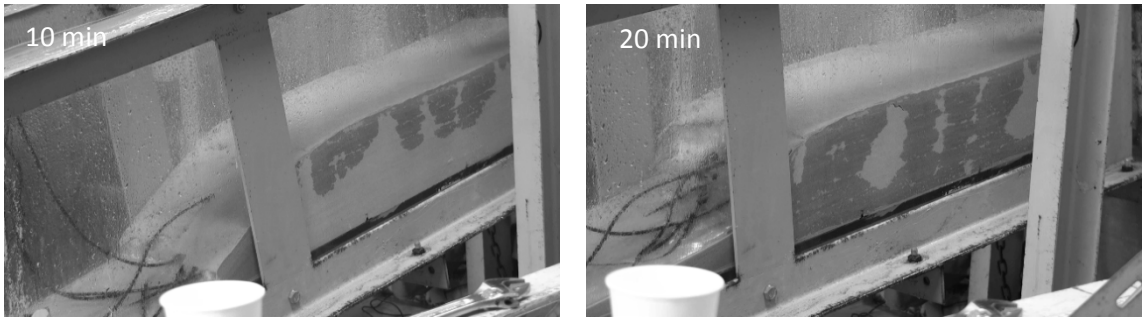

Figure 7: Time series data for flume experiment with 60% wettable sand and 40% water repellent sand. (a) Pore water pressure. (b) Volumetric water content. (c) Water and sand discharge at the bottom end of the flume. (d) Time-elapsed photographs oblique to the flume; light-dark color in sand denotes dry-saturated areas, respectively (sand height = 14.5 cm)

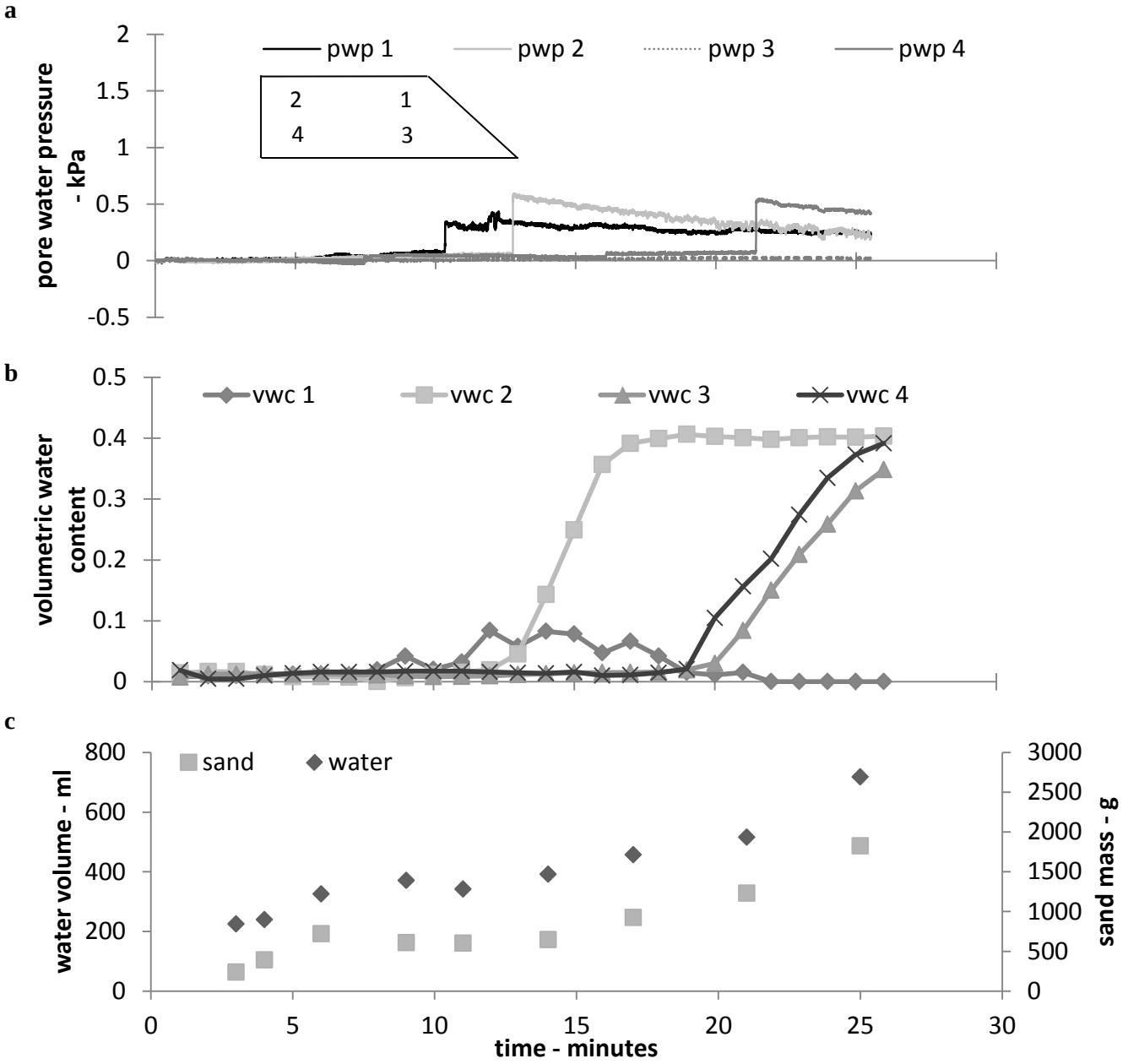
a
pwp 1
pwp 2
pwp 3
pwp 4
2
1
4
3
pore water pressure - kPa
2
1.5
1
0.5
0
-0.5
b
vwc 1
vwc 2
vwc 3
vwc 4
volumetric water content
0.5
0.4
0.3
0.2
0.1
0
c
sand
water
water volume - ml
800
600
400
200
0
3000
2500
2000
1500
1000
500
0
sand mass - g
0
5
10
15
20
25
30
time - minutes

d

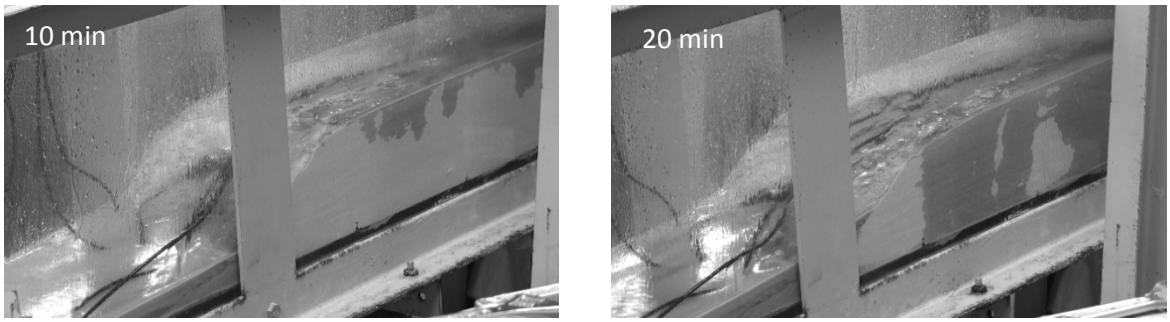

Figure 8: Time series data for flume experiment with 40% wettable sand and 60% water repellent sand. (a) Pore water pressure. (b) Volumetric water content. (c) Water and sand discharge at the bottom end of the flume. (d) Time-elapsed photographs oblique to the flume; light-dark color in sand denotes dry-saturated areas, respectively (sand height = 14.5 cm)

a

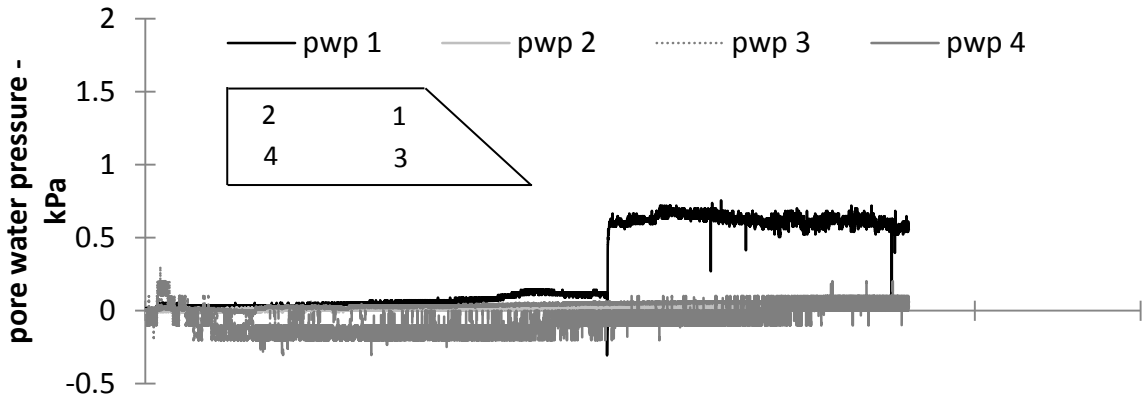
pwp 1
pwp 2
pwp 3
pwp 4
2
1
4
3
pore water pressure - kPa
2
1.5
1
0.5
0
-0.5

b

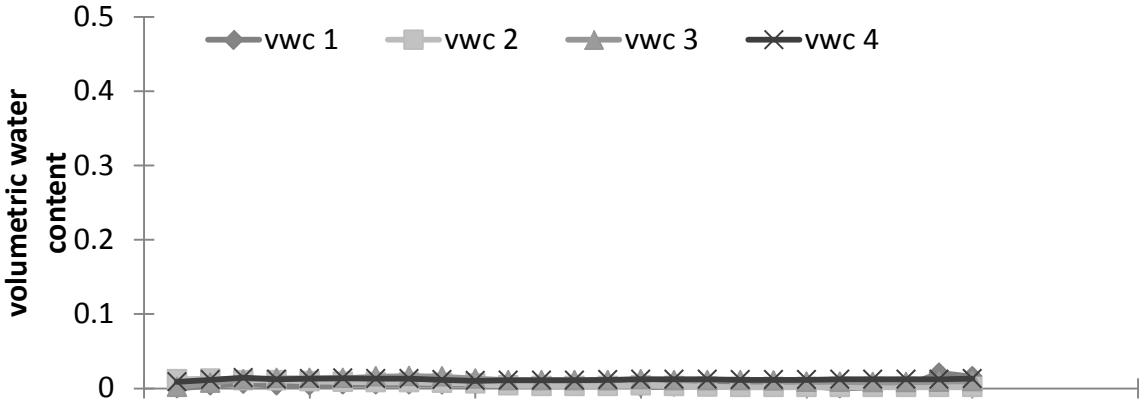
vwc 1
vwc 2
vwc 3
vwc 4
volumetric water content
0.5
0.4
0.3
0.2
0.1
0

c

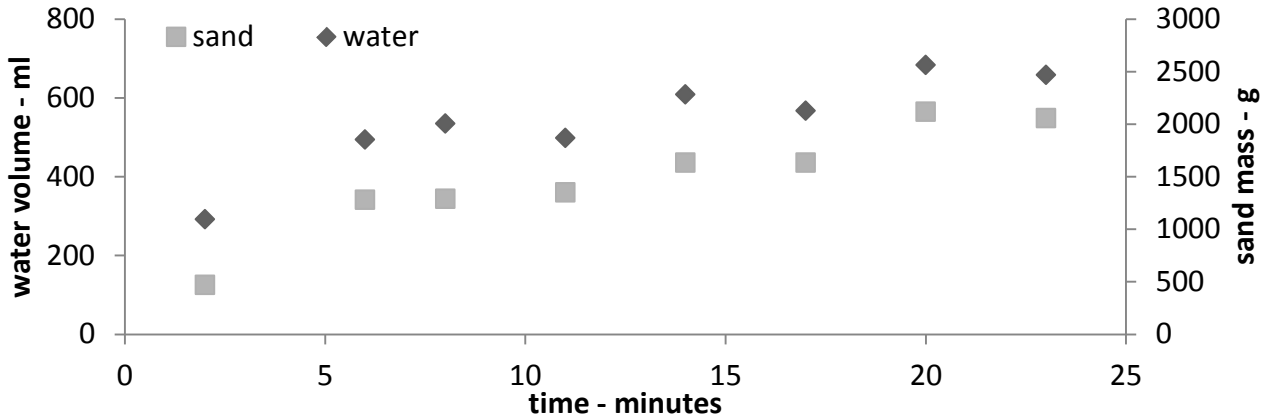
sand
water
water volume - ml
sand mass - g
800
600
400
200
0
3000
2500
2000
1500
1000
500
0
0
5
10
15
20
25
time - minutes

d

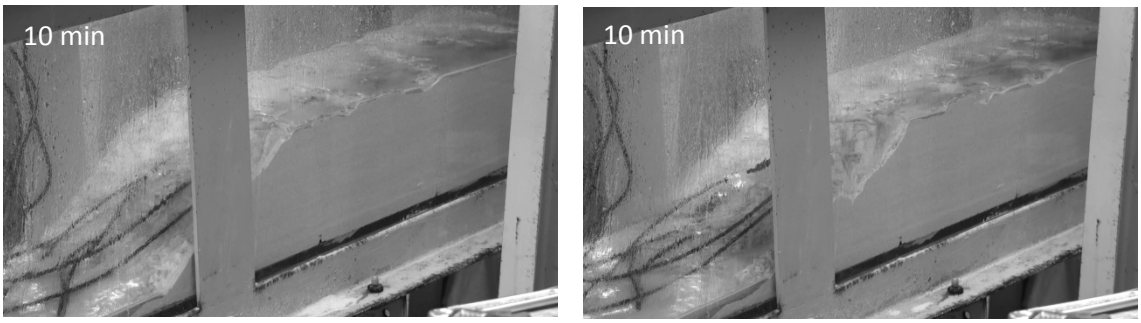

Figure 9: Time series data for flume experiment with 100% water repellent sand. (a) Pore water pressure. (b) Volumetric water content. (c) Water and sand discharge at the bottom end of the flume. (d) Time-elapsed photographs oblique to the flume; light-dark color in sand denotes dry-saturated areas, respectively (sand height = 14.5 cm)

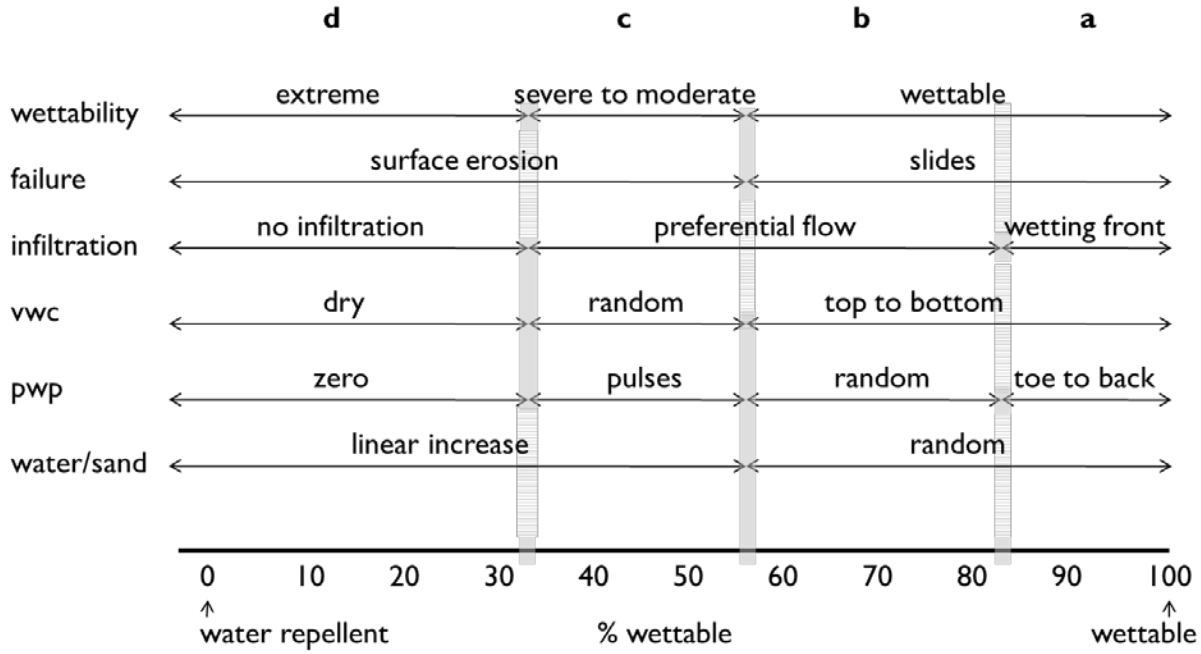

Figure 10: Model slope processes for the different mixtures, divided in four wettability classes (a, b, c, d) (pwp = pore water pressure, vwc = volumetric water content)

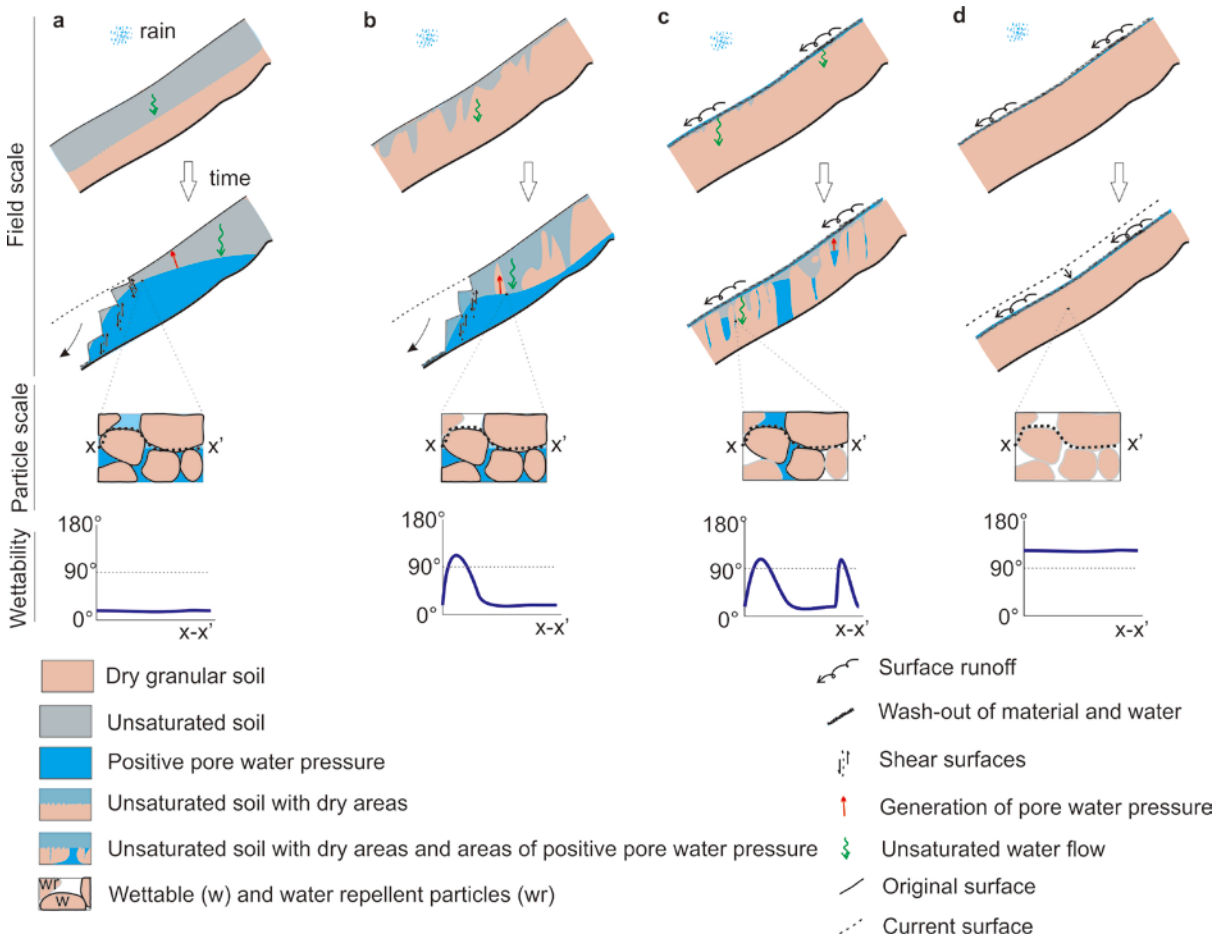

Figure 11: Simplified conceptual model for the initiation of debris flows triggered by rainfall for materials under variable wettability. (a) Wettable soil (contact angle ~0°). (b) Wettable soil (contact angle <90°). (c) Water repellent material (contact angle >90°, when in contact with water remains water repellent for a short period of time). (d) Water repellent material (contact angle >>90°, when in contact with water remains water repellent for a long period of time). Upper row denotes field conditions shortly after the rainfall onset. Middle row is for steady state conditions. Bottom row is on the interaction of meniscus and bulk water with wettable and water repellent particles.

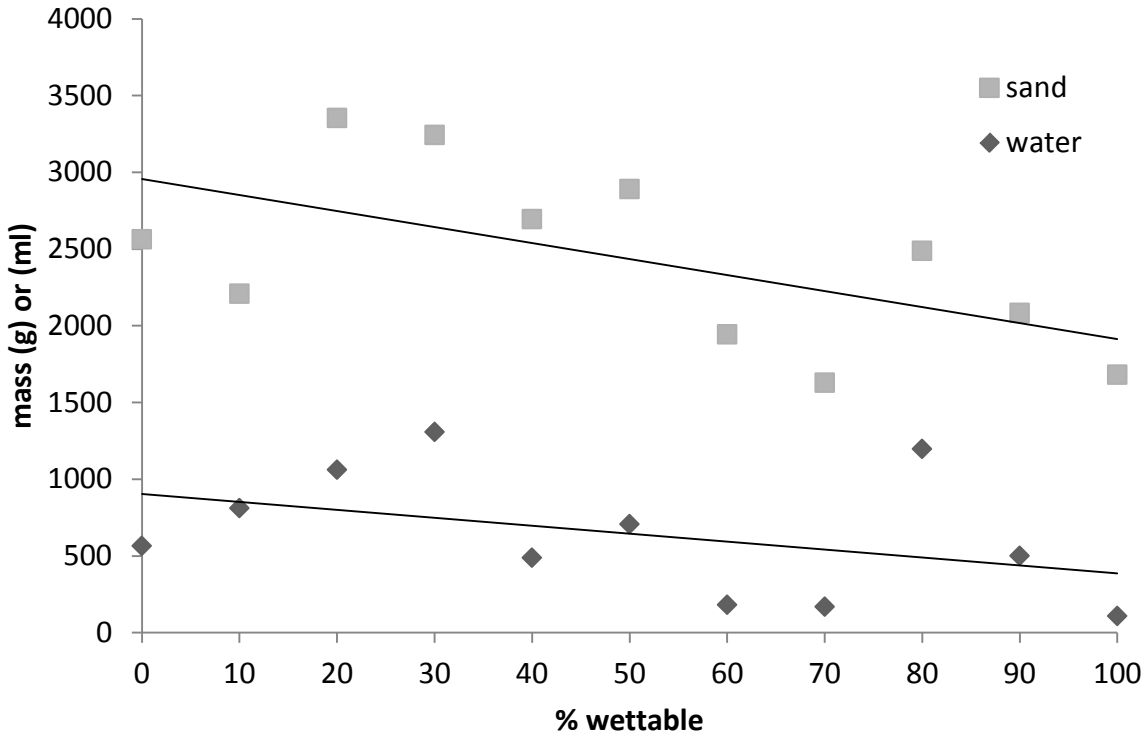

Figure 12: Peak water and sand discharge for the different mixtures